
State Representation Learning Using an Unbalanced Atlas

Li Meng¹, Morten Goodwin^{2,3}, Anis Yazidi^{3,4}, Paal Engelstad¹

¹University of Oslo

²Centre for Artificial Intelligence Research, University of Agder

³Oslo Metropolitan University

⁴Norwegian University of Science and Technology

Abstract

The manifold hypothesis posits that high-dimensional data often lies on a lower-dimensional manifold and that utilizing this manifold as the target space yields more efficient representations. While numerous traditional manifold-based techniques exist for dimensionality reduction, their application in self-supervised learning has witnessed slow progress. The recent MSIMCLR method combines manifold encoding with SimCLR but requires extremely low target encoding dimensions to outperform SimCLR, limiting its applicability. This paper introduces a novel learning paradigm using an unbalanced atlas (UA), capable of surpassing state-of-the-art self-supervised learning approaches. We meticulously investigated and engineered the DeepInfomax with an unbalanced atlas (DIM-UA) method by systematically adapting the Spatiotemporal DeepInfomax (ST-DIM) framework to align with our proposed UA paradigm, employing rigorous scientific methodologies throughout the process. The efficacy of DIM-UA is demonstrated through training and evaluation on the Atari Annotated RAM Interface (AtariARI) benchmark, a modified version of the Atari 2600 framework that produces annotated image samples for representation learning. The UA paradigm improves the existing algorithm significantly when the number of target encoding dimensions grows. For instance, the mean F1 score averaged over categories of DIM-UA is $\sim 75\%$ compared to $\sim 70\%$ of ST-DIM when using 16384 hidden units.

1 Introduction

Self-supervised learning (SSL) is a field in machine learning (ML) that aims to learn useful feature representations from unlabelled input data. SSL includes mainly contrastive methods [28, 5, 14] and generative models [18, 10, 27]. Generative models rely on using generative decoding and reconstruction loss, whereas typical contrastive methods do not involve a decoder but apply contrastive similarity metrics to hidden embeddings instead [23].

State representation learning (SRL) [2, 16, 22] focuses on learning representations from input data that are typically collected in a reinforcement learning (RL) environment. A collection of images can be sampled through an agent interacting with the environment according to a specified behavior policy. Such images are interesting as study subjects due to their innate temporal/spatial correlations. Moreover, RL can also benefit from self-supervised learning just as computer vision (CV) and natural language processing (NLP) do, and successful pretraining of neural network (NN) models can potentially lead to improvements in downstream RL tasks.

A manifold can be learned by finding an atlas that accurately describes the local structure in each chart [31]. In SSL, using an atlas can be viewed as a generalization of both dimensionality reduction and clustering [19, 20, 21]. Namely, it generalizes the case where only one chart exists and where the

charts do not overlap in an atlas. In practice, NNs can encode an atlas of a manifold by having chart embeddings and membership probabilities.

This work proposes a new SSL paradigm that takes advantage of an unbalanced atlas (UA), which means there is no uniform prior distribution, and the membership probability distribution is also not trained to be close to the uniform.

Our contribution is summarized as follows: (1) We modify the state-of-the-art SRL algorithm ST-DIM [2] with our UA paradigm and introduce a new algorithm called DIM-UA. (2) We compare DIM-UA with other SRL algorithms using samples collected from 19 Atari games of the AtariARI benchmark and illustrate that our algorithm achieves the best performance in terms of F1 scores and accuracy. (3) A detailed ablation study examines different underlying effects of possible design choices.

2 Related Work

Dimensionality reduction with manifolds It is common for nonlinear dimensionality reduction (NLDR) algorithms to approach their goals based on the manifold hypothesis. For example, the manifold structure of an isometric embedding can be discovered by solving for eigenvectors of the matrix of graph distances [33]. A sparse matrix can also be used instead with a locally linear embedding [32]. Correspondence between samples in different data sets can be recovered through the shared representations of the manifold [13]. Manifold regularization provides an out-of-sample extension to novel examples compared to graph-based approaches [3]. Manifold sculpting simulates surface tension progressively in local neighborhoods to discover manifolds [8].

Self-supervised learning There are some relevant works on generative models, such as variational autoencoders (VAEs) [18] and adversarial autoencoders (AAEs) [24]. Meanwhile, contrastive methods have shown promise in the field of SSL. Contrastive Predictive Coding (CPC) learns predictive representations based on the usefulness of the information in predicting future samples [28]. SimCLR provides a simple yet effective framework using data augmentations [5]. Momentum Contrast (MoCo) utilizes a dynamic dictionary, which can be much larger than the mini-batch size [14]. The recent trend within research in contrastive learning has been on removing the need for negative pairs. BYOL utilizes a momentum encoder to prevent the model from collapsing due to a lack of negative pairs [12]. SimSiam further shows that a stop-gradient operation alone is sufficient [6]. Barlow Twins, on the other hand, achieves so by minimizing the redundancy of vector components outputted by two identical networks that take distorted versions of inputs [36].

Self-supervised learning with manifolds Representing non-Euclidean data in NN models is a key topic in geometric deep learning [4]. Learning manifolds using NNs was explored in [19], in which AAEs were used to learn an atlas as latent parameters. Constant-curvature Riemannian manifolds (CCMs) of different curvatures can be learned similarly using AAEs [9]. Mixture models of VAEs can be used to express the charts and their inverses to solve inverse problems [1]. A combination of autoencoders and Barlow Twins can capture both the linear and nonlinear solution manifolds [17].

3 Method

We model a distribution of input data by a manifold as follows: x is the input from input space \mathcal{X} , \mathcal{Z} is the latent space, f is an embedding function: $\mathcal{X} \rightarrow \mathcal{Z}$. g_i is the identity mapping, d the number of dimensions for each chart output embedding, n the number of charts, and \mathcal{N} denotes $\{1, 2, \dots, n\}$. $\psi_i: \mathcal{Z} \rightarrow \mathbb{R}^d$ is the inverse mapping of a coordinate map: $\mathbb{R}^d \rightarrow \mathcal{Z}$, whereas $q = (q_1, q_2, \dots, q_n) : \mathcal{Z} \rightarrow [0, 1]^n$ is the chart membership function. The output of our model is then given by Eq. 1.

$$\text{Output}(x) = \sum q_i(f(x))g_i(\psi_i(f(x))) \tag{1}$$

At inference time, the one-hot encoding of $q(x)$ is used instead (Eq. 2).

$$\text{Output}(x) = g_i(\psi_i(f(x))), \text{ where } i = \operatorname{argmax}_j q_j(f(x)) \tag{2}$$

Like other SSL methods with manifolds [21, 20], UA also uses a maximal mean discrepancy (MMD) objective [11, 34], which is defined by Eq. 3.

$$\text{MMD}_k(P_1, P_2) = \left\| \int_{\mathcal{S}} k(s, \cdot) dP_1(s) - \int_{\mathcal{S}} k(s, \cdot) dP_2(s) \right\|_{\mathcal{H}_k} \quad (3)$$

Here, k is a reproducing kernel, \mathcal{H}_k is the reproducing kernel Hilbert space of real-valued functions mapping \mathcal{S} to \mathbb{R} , and P_1, P_2 are distributions on the space.

In our paradigm, the input x is designed to be represented in charts with higher membership probabilities. Thus, an MMD loss moves the conditional membership distribution far away from the uniform distribution. We use the kernel $k_{\mathcal{N}} : \mathcal{N} \times \mathcal{N} \rightarrow \mathbb{R}$, $(i, j) \rightarrow \delta_{ij}$, and $\delta_{ij} = 1$ if $i = j$ else 0, and thus have Eq. 4.

$$\mathcal{L}_{\mathcal{N}}(q) = -\mathbb{E}_z \text{MMD}_{k_{\mathcal{N}}}(q(z), \mathcal{U}_{\mathcal{N}}) = -\mathbb{E}_z \sum_{i=1}^n \left(q_i(z) - \frac{1}{n} \right)^2 \quad (4)$$

Here, $\mathcal{U}_{\mathcal{N}}$ denotes the uniform distribution on \mathcal{N} , z is the embedding of $f(x)$.

Unlike MSIMCLR [21], we do not use an MMD objective to make the prior distribution to be uniform. We hypothesize that, although making the prior uniform can represent the data distribution more efficiently when d is extremely small, it suffers from a similar problem as bootstrapped methods in RL. It has been pointed out that multiple NN heads inside a model, in the absence of additional noise, tend to output similar results after being trained a large number of epochs [30, 29, 7, 26]. Forcing a uniform prior distribution when d is reasonably large can lead to low diversity among charts as well.

Instead of using a uniform prior, we take another approach to improve the model stability and head diversity when d is large. First, an illustration of a manifold Z is shown in Figure 1. Two domains are denoted by U_{α} and U_{β} in Z . ψ_{α} and ψ_{β} are the corresponding charts in the atlas that map them to a lower dimensional Euclidean space. The intersection $U_{\alpha} \cap U_{\beta}$ has transitive maps in their respective chart coordinates with domains restricted to $\psi_{\alpha}(U_{\alpha} \cap U_{\beta})$ and $\psi_{\beta}(U_{\alpha} \cap U_{\beta})$, which are $\psi_{\alpha\beta} = \psi_{\beta} \circ \psi_{\alpha}^{-1}$ and $\psi_{\beta\alpha} = \psi_{\alpha} \circ \psi_{\beta}^{-1}$.

What interests us the most is this intersection between U_{α} and U_{β} . More precisely, since the overlapping representations in each head of the model become a dominant negative factor when d grows large, we aim at modelling a manifold with a dilated prediction target to avoid convergent head embeddings and collapsing solutions. We use the average values of chart outputs to model a Minkowski sum [25, 35], which serves a key purpose in our paradigm.

Proposition 1. *Let $U = \{U_1, U_2, \dots, U_n\}$ be a collection of open subsets of Z whose union is all of Z , and $\bigcap_{i=1}^n U_i$ is not empty. For each $i \in \{1, 2, \dots, n\}$, there is a homeomorphism $\psi_i : U_i \rightarrow V_i$ to an open set $V_i \subset \mathbb{R}^d$. We have the Minkowski sum $V_i + V_j = \{a + b \mid a \in V_i, b \in V_j\}$. Then $\sum_{i=1}^n \psi_i \left(\bigcap_{j=1}^n U_j \right) \subset \sum_{i=1}^n V_i$.*

Proof. For any vector $a \in \sum_{i=1}^n \psi_i \left(\bigcap_{j=1}^n U_j \right)$, there exists $a_i \in \psi_i \left(\bigcap_{j=1}^n U_j \right)$ such that $a = \sum_{i=1}^n a_i$.

Because $\psi_i \left(\bigcap_{j=1}^n U_j \right) \subset V_i$, we also have $a_i \in V_i$, $i \in \{1, 2, \dots, n\}$. Then $\sum_{i=1}^n a_i \in \sum_{i=1}^n V_i$, $a \in \sum_{i=1}^n V_i$ and thus $\sum_{i=1}^n \psi_i \left(\bigcap_{j=1}^n U_j \right) \subset \sum_{i=1}^n V_i$. □

Proposition 2. *Let $U = \{U_1, U_2, \dots, U_n\}$ be a collection of open subsets of Z whose union is all of Z , and $\bigcap_{i=1}^n U_i$ is not empty. For each $i \in \{1, 2, \dots, n\}$, there is a homeomorphism $\psi_i : U_i \rightarrow V_i$ to an*

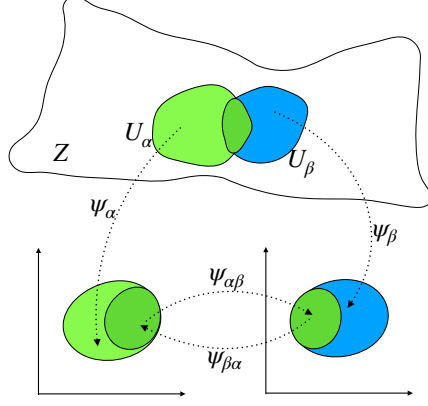


Figure 1: A manifold Z embedded in a higher dimension.

open set $V_i \subset \mathbb{R}^d$. The multiplication of set V and a scalar λ is defined to be $\lambda V = \{\lambda a \mid a \in V\}$. We take the Minkowski sum. If each $\psi_i(\prod_{j=1}^n U_j)$ is convex, then $\sum_{i=1}^n \frac{1}{n} \psi_i(\prod_{j=1}^n U_j) \subset \frac{1}{n} \sum_{i=1}^n V_i$.

Proof. Follows Proposition 1 and the property of scalar multiplication, $\frac{1}{n} \sum_{i=1}^n \psi_i(\prod_{j=1}^n U_j) \subset \frac{1}{n} \sum_{i=1}^n V_i$. Since scalar multiplication is preserved for convex sets, we have $\sum_{i=1}^n \frac{1}{n} \psi_i(\prod_{j=1}^n U_j) \subset \frac{1}{n} \sum_{i=1}^n V_i$. □

We experiment with our UA paradigm using the SRL algorithm ST-DIM [2], and propose DIM-UA. ST-DIM develops on Deep InfoMax (DIM)[15] that uses infoNCE [28] as the mutual information estimator between patches. Its objective consists of two components. One is the global-local objective (\mathcal{L}_{GL}) and the other one is the local-local objective (\mathcal{L}_{LL}), defined by Eq. 5 and Eq. 6 respectively.

$$\mathcal{L}_{GL} = \sum_{m=1}^M \sum_{n=1}^N -\log \frac{\exp(g_{m,n}(x_t, x_{t+1}))}{\sum_{x_{t*} \in X_{next}} \exp(g_{m,n}(x_t, x_{t*}))} \quad (5)$$

$$\mathcal{L}_{LL} = \sum_{m=1}^M \sum_{n=1}^N -\log \frac{\exp(h_{m,n}(x_t, x_{t+1}))}{\sum_{x_{t*} \in X_{next}} \exp(h_{m,n}(x_t, x_{t*}))} \quad (6)$$

Here, x_t and x_{t+1} are temporally adjacent observations, whereas X_{next} is the set of next observations and x_{t*} is randomly sampled from the minibatch. M and N are the height and width of local feature representations. We denote the encoder as θ and the local feature vector of the input x_t at the point (m, n) as $\theta_{m,n}(x_t)$. Then, we have the score function $g_{m,n}(x_t, x_{t+1}) = \theta(x_t)^T W_g \theta_{m,n}(x_{t+1})$, and $h_{m,n}(x_t, x_{t+1}) = \theta_{m,n}(x_t)^T W_h \theta_{m,n}(x_{t+1})$.

We redefine the score function of \mathcal{L}_{GL} of DIM-UA as in Eq. 7 using the UA paradigm.

$$g_{m,n}(x_t, x_{t+1}) = \left[\frac{1}{n} \sum_{i=1}^n \theta_i(x_t) \right]^T W_g \theta_{m,n}(x_{t+1}) \quad (7)$$

Here, $\theta_i(x_t)$ is the output of x_t from the i -th head of the encoder θ for each i in \mathcal{N} .

Table 1: The values of hyper-parameters

Hyper-parameter	Value
Image size	160×210
Minibatch size	64
Learning rate	$3e-4$
Epochs	100
Pretraining steps	80000
Probe training steps	35000
Probe testing steps	10000

We have the MMD objective \mathcal{L}_Q defined by Eq. 8, where $\theta_{q_i}(x_t)$ is the membership probability of the i -th head for each i in \mathcal{N} when the input is x_t .

$$\mathcal{L}_Q = -\frac{1}{2} \sum_{i=1}^n \left((\theta_{q_i}(x_t) - \frac{1}{n})^2 + (\theta_{q_i}(x_{t+1}) - \frac{1}{n})^2 \right) \quad (8)$$

Thereby, the UA objective (Eq. 9) is a sum of the above objectives, where τ is a hyper-parameter.

$$\mathcal{L}_{UA} = \mathcal{L}_{GL} + \mathcal{L}_{LL} + \tau \mathcal{L}_Q \quad (9)$$

The output of the encoder follows Eq. 1 and Eq. 2, which can be written as $\theta(x_t) = \sum \theta_{q_i}(x_t) \theta_i(x_t)$, and at inference time, $\theta(x_t) = \theta_i(x_t)$, where $i = \operatorname{argmax}_j \theta_{q_j}(x_t)$.

4 Experimental Details

The performance of DIM-UA and other SRL methods is evaluated on the 19 games of the AtariARI benchmark. There are five categories of state variables in AtariARI [2], which are agent localization (Agent Loc.), small object localization (Small Loc.), other localization (Other Loc.), miscellaneous (Misc.), and score/clock/lives/display (Score/.../Display).

We follow the customary SSL pipeline and record the probe accuracy and F1 scores on the downstream linear probing tasks. The encoder is first pretrained with SSL, and then is used to predict the ground truth of an image with an additional linear classifier. Notably, the weights of the encoder are trained only during the pretraining and are fixed in the probing tasks. The data for pretraining and probing are collected by an RL agent running a certain number of steps using a random policy since it was found that the samples collected by a random policy could be more favorable than those collected by policy gradient policies for the SSL methods [2].

Table 1 provides the values of some crucial hyper-parameters that are kept the same across different methods. For DIM-UA, τ is set to 0.1.

Previous SSL methods in [2] have used a single output head with 256 hidden units. One of the major interests in our experiment is to discover the effect of choosing different values for d and n . Therefore, we scale up the number of hidden units, while keeping the model architecture, to observe the performance of using a single output head without UA and of using multiple heads with UA. To make a fair comparison, we compare the performance when the total number of hidden units are equal, i.e., when $1 \times d$ for a single output head and $n \times d$ for multiple output heads are equal. As an example, a model with a single output head of 1024 units is compared to 4 heads of 256 hidden units in our experiment. In contrast, MSIMCLR compares the results of different methods with d being equal [21], which gives using multiple heads an additional advantage.

5 Results

In this section, we show the empirical results of our experiment. In particular, we are interested in comparing DIM-UA with other SSL methods to verify the efficacy of our UA paradigm. Meanwhile, we pay special attention to the performance when choosing different values for n and d .

For a straightforward comparison, we first include the results of ST-DIM with one output head of 16384 units (ST-DIM*) and DIM-UA with four output heads of 4096 units. We compare them to the

results of using a single output head with 256 hidden units, which are taken from [2]. The probe F1 scores of each game averaged across categories are shown in Table 2. The probe accuracy scores are shown in Table 3. Each table entry is an average of 5 independent pretraining/probing runs using images sampled from different seeds.

First, using 16384 units (ST-DIM*) does not necessarily guarantee better performance than using 256 units (ST-DIM). In 7 out of 19 games, ST-DIM* has lower F1 scores than ST-DIM. In particular, the model collapses due to overfitting when using too many units to represent the global features on Freeway. As a result, the mean F1 score of ST-DIM* is only 0.7 compared to 0.72 for ST-DIM, and the accuracy is 0.71 compared to 0.73. On the other hand, DIM-UA shows higher scores and more stable performance. The F1 scores and accuracy of DIM-UA are equal or higher than those of ST-DIM* and ST-DIM in every game. The mean F1 score of DIM-UA is 0.75, and the mean accuracy is 0.76, the highest among different methods in Table 2 and Table 3.

A detailed examination of using different numbers of hidden units is shown in Fig. 2. ST-DIM performs better than DIM-UA when the number of hidden units is small. Their performances become close to each other when the number of units is around 2048. DIM-UA continues to improve while the number of units grows, whereas the performance of ST-DIM drops at the same time. It is expected for DIM-UA to have lower F1 scores and accuracy when the encoding dimensions are low since the diversity among output heads demands more epochs of training. However, the efficacy of our UA paradigm is clearly demonstrated, as it allows the model to extend its capability by continuously expanding the encoding dimensions.

Since we expect DIM-UA to converge slower because of the diversity among output heads, we expect this to become more obvious as the number of heads increases. We can verify that in Fig. 3, where average results of heads from 6 games (i.e., Asteroids, Breakout, Montezuma Revenge, Private Eye, Seaquest, Video Pinball) are used to perform an ablation study. We can see that the model with two output heads has the highest F1 score and accuracy when the total number of hidden units is below 2048. On the other hand, it obtains the lowest F1 score and accuracy when the total number of units grows to 16384. However, the model with eight output heads gives the worst results when the number of units is small but shows no sign of plateau, even with very high encoding dimensions. Increasing n while keeping d the same in our UA paradigm helps with the manifold representation but also lowers the model’s performance if d is not large enough.

In addition, we compare DIM-UA with two other methods modified on ST-DIM using the same six games in Fig. 4. One uses the paradigm from MSIMCLR, denoted by "+MMD". The other is similar to ours but does not use a surrogate prediction target, i.e., not using Eq. 7, denoted by "-UA". It is not surprising that "+MMD" obtains the worst results in spite of the number of units since MSIMCLR was only found out to be helpful when the number of units is extremely small (e.g., 2, 4). "-UA" obtains better results than DIM-UA when the number of units is 512 but gets overrun by DIM-UA when the number becomes larger. This empirically demonstrates that the surrogate prediction target in our UA paradigm is critical to achieve efficient manifold representations.

6 Discussion

We have demonstrated that our UA paradigm helps improve the performance of ST-DIM when encoding dimensions are high. However, the performance deteriorates when dimensions are low. We argue that training NNs with multiple output heads is inherently slower and more demanding than training with a single output head, which has restrained the study in its domain. MSIMCLR bypasses this issue by comparing, for example, using four heads with eight units each (32 units in total) to using one head with eight units [21]. With high encoding dimensions, our method does not escape from this quandary, yet achieves significantly better results than using a single output head. Thus, it is evident that our paradigm can overcome the headwind by generating effective manifold representations.

Notably, the UA paradigm also exhibits the potential of modelling a manifold using further higher dimensions while increasing the number of output heads in Fig. 3. It can be an important contribution because this means the performance of the model scale with the size of output heads. Using 16384 hidden units in output heads is not very efficient economically when the entire model is small, but the additional overhead introduced by doing so can be relatively insignificant when the model itself is

Table 2: Probe F1 scores of each game averaged across categories

Game	VAE	PIXEL-PRED	CPC	ST-DIM	ST-DIM*	DIM-UA
Asteroids	0.36	0.34	0.42	0.49	0.48	0.5
Bowling	0.50	0.81	0.90	0.96	0.96	0.96
Boxing	0.20	0.44	0.29	0.58	0.61	0.64
Breakout	0.57	0.70	0.74	0.88	0.88	0.9
Demon Attack	0.26	0.32	0.57	0.69	0.71	0.74
Freeway	0.01	0.81	0.47	0.81	0.3	0.86
Frostbite	0.51	0.72	0.76	0.75	0.73	0.75
Hero	0.69	0.74	0.90	0.93	0.93	0.94
Montezuma Revenge	0.38	0.74	0.75	0.78	0.81	0.84
Ms Pacman	0.56	0.74	0.65	0.72	0.74	0.76
Pitfall	0.35	0.44	0.46	0.60	0.69	0.73
Pong	0.09	0.70	0.71	0.81	0.78	0.85
Private Eye	0.71	0.83	0.81	0.91	0.91	0.93
Qbert	0.49	0.52	0.65	0.73	0.78	0.79
Seaquest	0.56	0.62	0.66	0.67	0.68	0.69
Space Invaders	0.52	0.57	0.54	0.57	0.59	0.62
Tennis	0.29	0.57	0.60	0.60	0.57	0.64
Venture	0.38	0.46	0.51	0.58	0.57	0.58
Video Pinball	0.45	0.57	0.58	0.61	0.6	0.62
Mean	0.41	0.61	0.63	0.72	0.7	0.75

Table 3: Probe accuracy scores of each game averaged across categories

Game	VAE	PIXEL-PRED	CPC	ST-DIM	ST-DIM*	DIM-UA
Asteroids	0.41	0.43	0.48	0.52	0.51	0.53
Bowling	0.56	0.83	0.90	0.96	0.96	0.96
Boxing	0.23	0.45	0.32	0.59	0.61	0.64
Breakout	0.61	0.71	0.75	0.89	0.89	0.91
Demon Attack	0.31	0.35	0.58	0.70	0.72	0.74
Freeway	0.07	0.85	0.49	0.82	0.33	0.86
Frostbite	0.54	0.72	0.76	0.75	0.73	0.75
Hero	0.72	0.75	0.90	0.93	0.93	0.94
Montezuma Revenge	0.41	0.74	0.76	0.78	0.81	0.84
Ms Pacman	0.60	0.75	0.67	0.73	0.75	0.77
Pitfall	0.35	0.47	0.49	0.61	0.7	0.74
Pong	0.19	0.72	0.73	0.82	0.79	0.85
Private Eye	0.72	0.83	0.81	0.91	0.91	0.93
Qbert	0.53	0.54	0.66	0.74	0.79	0.8
Seaquest	0.61	0.65	0.69	0.69	0.69	0.7
Space Invaders	0.57	0.61	0.57	0.59	0.6	0.63
Tennis	0.37	0.59	0.61	0.61	0.58	0.65
Venture	0.43	0.48	0.52	0.59	0.58	0.59
Video Pinball	0.47	0.58	0.59	0.61	0.6	0.63
Mean	0.46	0.63	0.65	0.73	0.71	0.76

huge. In particular, this trade-off may also be worthwhile in downstream tasks where the smallest increase in probe accuracy can make a difference.

7 Conclusion

We present our UA paradigm for representation learning using an unbalanced atlas and design a new SRL method based on the UA paradigm. We demonstrate that our paradigm improves the state-of-the-art SRL methods significantly by following the SSL experimental pipeline and comparing the probe F1 scores and accuracy. Ablation study shows that the new surrogate prediction target is

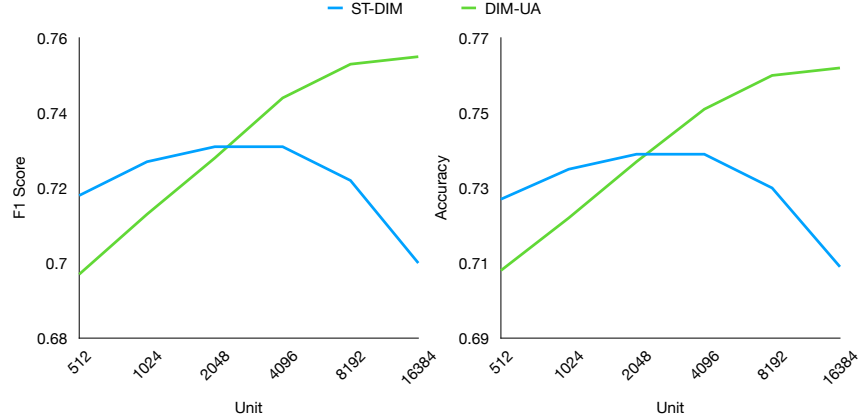


Figure 2: The mean F1 score and accuracy of 19 games when choosing different total numbers of hidden units. The number of heads of DIM-UA is 4 in this figure. The number of units in each head of DIM-UA is the total number divided by 4, e.g., 4×1024 when the value in the horizontal axis is 4096.

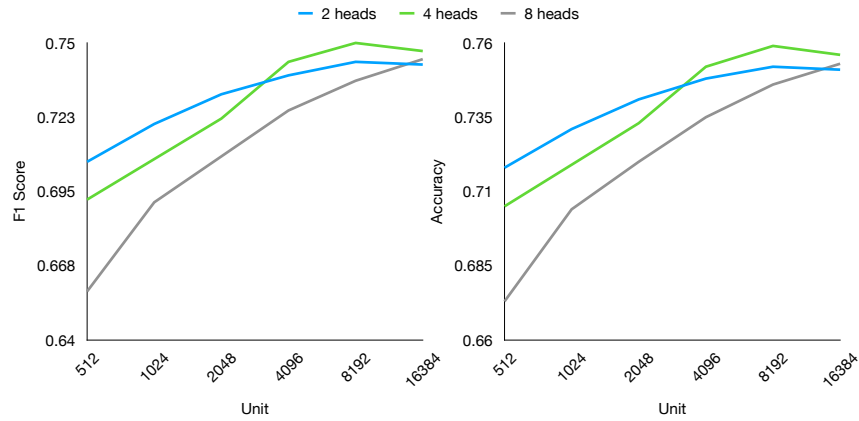


Figure 3: The mean F1 score and accuracy of 6 games when choosing different total numbers of hidden units for DIM-UA. Likewise, the number of units in each head is the total number divided by the number of heads, e.g., 2×2048 , 4×1024 , 8×512 when 4096 units.

important in achieving state-of-the-art results. Using more output heads in our model and increasing the total number of hidden units is also possible.

Our work has illustrated that SSL methods with manifolds have great potential, and more topics can be researched in this area. Although large models can benefit from our paradigm easily, it is not feasible to infinitely increase the number of hidden units in output heads in an NN model. Future research should focus on representing a manifold using an unbalanced atlas more efficiently, e.g., designing new objectives and constraints.

Acknowledgments

This work was performed on the [ML node] resource, owned by the University of Oslo, and operated by the Department for Research Computing at USIT, the University of Oslo IT-department. <http://www.hpc.uio.no/>

References

- [1] G. S. Alberti, J. Hertrich, M. Santacesaria, and S. Sciutto. Manifold learning by mixture models of vaes for inverse problems. *arXiv preprint arXiv:2303.15244*, 2023.

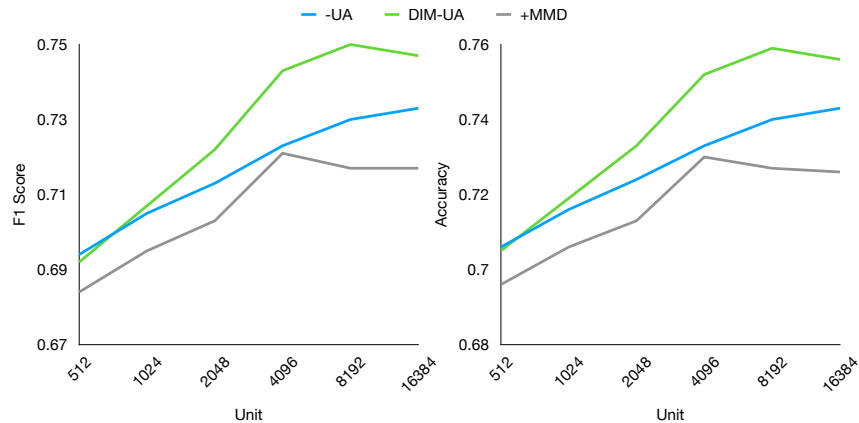


Figure 4: The mean F1 score and accuracy of 6 games with different settings. All settings use 4 output heads. The total number of units (in the horizontal axis) is the number of hidden units in each head multiplied by 4.

- [2] A. Anand, E. Racah, S. Ozair, Y. Bengio, M.-A. Côté, and R. D. Hjelm. Unsupervised state representation learning in atari. *Advances in neural information processing systems*, 32, 2019.
- [3] M. Belkin, P. Niyogi, and V. Sindhwani. Manifold regularization: A geometric framework for learning from labeled and unlabeled examples. *Journal of machine learning research*, 7(11), 2006.
- [4] M. M. Bronstein, J. Bruna, Y. LeCun, A. Szlam, and P. Vandergheynst. Geometric deep learning: going beyond euclidean data. *IEEE Signal Processing Magazine*, 34(4):18–42, 2017.
- [5] T. Chen, S. Kornblith, M. Norouzi, and G. Hinton. A simple framework for contrastive learning of visual representations. In *International conference on machine learning*, pages 1597–1607. PMLR, 2020.
- [6] X. Chen and K. He. Exploring simple siamese representation learning. In *Proceedings of the IEEE/CVF conference on computer vision and pattern recognition*, pages 15750–15758, 2021.
- [7] A. Ecoffet, J. Huizinga, J. Lehman, K. O. Stanley, and J. Clune. Go-explore: a new approach for hard-exploration problems. *arXiv preprint arXiv:1901.10995*, 2019.
- [8] M. Gashler, D. Ventura, and T. Martinez. Iterative non-linear dimensionality reduction with manifold sculpting. *Advances in neural information processing systems*, 20, 2007.
- [9] D. Grattarola, L. Livi, and C. Alippi. Adversarial autoencoders with constant-curvature latent manifolds. *Applied Soft Computing*, 81:105511, 2019.
- [10] K. Gregor, I. Danihelka, A. Graves, D. Rezende, and D. Wierstra. Draw: A recurrent neural network for image generation. In *International conference on machine learning*, pages 1462–1471. PMLR, 2015.
- [11] A. Gretton, K. M. Borgwardt, M. J. Rasch, B. Schölkopf, and A. Smola. A kernel two-sample test. *The Journal of Machine Learning Research*, 13(1):723–773, 2012.
- [12] J.-B. Grill, F. Strub, F. Altché, C. Tallec, P. Richemond, E. Buchatskaya, C. Doersch, B. Avila Pires, Z. Guo, M. Gheshlaghi Azar, et al. Bootstrap your own latent—a new approach to self-supervised learning. *Advances in neural information processing systems*, 33:21271–21284, 2020.
- [13] J. H. Ham, D. D. Lee, and L. K. Saul. Learning high dimensional correspondences from low dimensional manifolds. *International Conference on Machine Learning Workshop*, 2003.
- [14] K. He, H. Fan, Y. Wu, S. Xie, and R. Girshick. Momentum contrast for unsupervised visual representation learning. In *Proceedings of the IEEE/CVF conference on computer vision and pattern recognition*, pages 9729–9738, 2020.
- [15] R. D. Hjelm, A. Fedorov, S. Lavoie-Marchildon, K. Grewal, P. Bachman, A. Trischler, and Y. Bengio. Learning deep representations by mutual information estimation and maximization. *arXiv preprint arXiv:1808.06670*, 2018.
- [16] R. Jonschkowski and O. Brock. Learning state representations with robotic priors. *Autonomous Robots*, 39(3):407–428, 2015.
- [17] T. Kadeethum, F. Ballarin, D. O’malley, Y. Choi, N. Bouklas, and H. Yoon. Reduced order modeling for flow and transport problems with barlow twins self-supervised learning. *Scientific Reports*, 12(1):20654, 2022.
- [18] D. P. Kingma and M. Welling. Auto-encoding variational bayes. *arXiv preprint arXiv:1312.6114*, 2013.

- [19] E. O. Korman. Autoencoding topology. *arXiv preprint arXiv:1803.00156*, 2018.
- [20] E. O. Korman. Atlas based representation and metric learning on manifolds. *arXiv preprint arXiv:2106.07062*, 2021.
- [21] E. O. Korman. Self-supervised representation learning on manifolds. In *ICLR 2021 Workshop on Geometrical and Topological Representation Learning*, 2021.
- [22] T. Lesort, N. Díaz-Rodríguez, J.-F. Goudou, and D. Filliat. State representation learning for control: An overview. *Neural Networks*, 108:379–392, 2018.
- [23] X. Liu, F. Zhang, Z. Hou, L. Mian, Z. Wang, J. Zhang, and J. Tang. Self-supervised learning: Generative or contrastive. *IEEE Transactions on Knowledge and Data Engineering*, 35(1):857–876, 2021.
- [24] A. Makhzani, J. Shlens, N. Jaitly, I. Goodfellow, and B. Frey. Adversarial autoencoders. *arXiv preprint arXiv:1511.05644*, 2015.
- [25] M. Mamatov and J. Nuritdinov. Some properties of the sum and geometric differences of minkowski. *Journal of Applied Mathematics and Physics*, 8(10):2241–2255, 2020.
- [26] L. Meng, M. Goodwin, A. Yazidi, and P. Engelstad. Improving the diversity of bootstrapped dqn by replacing priors with noise. *IEEE Transactions on Games*, 2022.
- [27] J. Oh, X. Guo, H. Lee, R. L. Lewis, and S. Singh. Action-conditional video prediction using deep networks in atari games. *Advances in neural information processing systems*, 28, 2015.
- [28] A. v. d. Oord, Y. Li, and O. Vinyals. Representation learning with contrastive predictive coding. *arXiv preprint arXiv:1807.03748*, 2018.
- [29] I. Osband, C. Blundell, A. Pritzel, and B. Van Roy. Deep exploration via bootstrapped dqn. *Advances in neural information processing systems*, 29:4026–4034, 2016.
- [30] I. Osband and B. Van Roy. Bootstrapped thompson sampling and deep exploration. *arXiv preprint arXiv:1507.00300*, 2015.
- [31] N. Pitelis, C. Russell, and L. Agapito. Learning a manifold as an atlas. In *Proceedings of the IEEE Conference on Computer Vision and Pattern Recognition*, pages 1642–1649, 2013.
- [32] S. T. Roweis and L. K. Saul. Nonlinear dimensionality reduction by locally linear embedding. *science*, 290(5500):2323–2326, 2000.
- [33] J. B. Tenenbaum, V. d. Silva, and J. C. Langford. A global geometric framework for nonlinear dimensionality reduction. *science*, 290(5500):2319–2323, 2000.
- [34] I. Tolstikhin, O. Bousquet, S. Gelly, and B. Schoelkopf. Wasserstein auto-encoders. *arXiv preprint arXiv:1711.01558*, 2017.
- [35] X. Wang, J. Zhang, and W. Zhang. The distance between convex sets with minkowski sum structure: application to collision detection. *Computational Optimization and Applications*, 77:465–490, 2020.
- [36] J. Zbontar, L. Jing, I. Misra, Y. LeCun, and S. Deny. Barlow twins: Self-supervised learning via redundancy reduction. In *International Conference on Machine Learning*, pages 12310–12320. PMLR, 2021.